Soft-X-ray spectra of highly charged Au ions in an electron-beam ion trap

E. Träbert, P. Beiersdorfer, K.B. Fournier, S.B. Utter, and K.L. Wong

Abstract: Systematic variation of the electron-beam energy in an electron-beam ion trap has been employed to produce soft-X-ray spectra (20 to 60 Å) of Au with well-defined maximum charge states ranging from Br- to Co-like ions. Guided by large-scale relativistic atomic structure calculations, the strongest $\Delta n = 0$ ($n = 4$ to $n' = 4$) transitions in Rb- to Cu-like ions (Au^{42+} – Au^{50+}) have been identified.

PACS Nos.: 32.30Rj, 39.30+w, 31.50+w, 32.20R

Résumé : Nous avons varié systématiquement l'énergie des électrons dans un piège ionique à faisceau électronique afin de produire le spectre X mou de Au (de 20 à 60 Å) avec des états de charge ionique la plus élevée et bien définis comme étant les ions isoélectroniques allant du Br au Co. À la lumière de calculs relativistes à grande échelle pour la structure électronique, nous avons identifié les plus fortes transitions $\Delta n = 0$ ($n = 4$ à $n' = 4$) dans les ions Au^{42+} – Au^{50+} qui sont isoélectroniques aux éléments allant du Rb au Cu.

1. Introduction

Energetic, hot plasmas can be produced by various means from controlled fusion experiments based on tokamak discharges [1, 2]; by high-power laser irradiation of a solid [3, 4]; or, as has also been proposed, by intense ion beams striking a fuel pellet. To analyze the plasma conditions reached, one needs to identify characteristic spectral lines that reveal the presence of specific highly charged ions, evaluate relative line intensities for collisional-radiative modeling efforts, or measure line widths for deriving an ion temperature.

For a while, the highest charge state ions were observed in laser-produced plasmas. However, for a number of isoelectronic sequences the wavelengths obtained from these plasmas did not sustain the isoelectronic trends of lower nuclear charge Z ions observed in less powerful light sources, nor trends predicted in calculated data. After calculations had improved considerably and seemed to account well for the massive relativistic effects in high-Z ions [5], hypotheses were brought forward on mass motion effects that may have corrupted the wavelengths in some of the laser-plasma experiments. The Doppler effect poses comparable problems for precise wavelength measurements on fast ion beams. Although procedures have been developed to correct for the Doppler effect of fast ion beams, and although ions in all charge states are amenable to beam-foil spectroscopy in principle [6], the necessary effort has precluded any wide-range survey work on very highly charged heavy ions.

Received June 7, 2000. Accepted November 19, 2000. Published on the NRC Research Press Web site on May 2, 2001.

E. Träbert,[1] P. Beiersdorfer, K.B. Fournier, S.B. Utter, and K.L. Wong. Physics Division, Lawrence Livermore National Laboratory, Livermore, CA 94550-9234, U.S.A.

[1] Permanent address: Fakultät für Physik und Astronomie, Ruhr-Universität Bochum, D-44780 Bochum, Germany. e-mail: (traebert@ep3.ruhr-uni-bochum.de).

 DOI: 10.1139/cjp-79-2/3-153

Recently, another light source has become available, the electron-beam ion trap (EBIT) [7]. In this device the ions are practically at rest, and accurate wavelength measurements are feasible without any Doppler shifts. Also, as ionization and excitation proceed in a stepwise fashion, the electron-beam energy determines the highest charge state that can be produced. By adjusting that energy, spectral lines of ions of a single charge state can be added to a spectrum that has been recorded at lower energy. Hence, systematic work becomes possible that identifies spectral lines by element and production threshold (the ionization potential of the next lower ionization stage). This process is demonstrated here with the soft-X-ray spectrum of Rb- to Cu-like ions of Au ($Z = 79$). Companion studies measure similar data from W ($Z = 74$) as well as isoelectronic trends in Cu-like lines in elements from Yb to U[2] and from the adjacent X-ray range spectra of Au.[3] Au plays an important role as an inner wall material of hohlraums in inertial confinement fusion (ICF) research with indirect drive [8,9]. In that approach, irradiation with laser light produces intense Au X-rays that drive the implosion. Au has also been seen in such plasmas as an impurity introduced by the incidental erosion of antenna surfaces. Data on Au are also essential to tokamak fusion experiments as they serve as a cross check of the findings on W, an element used for surfaces that are exposed to the plasma in heat-bearing divertor structures in magnetically confined fusion experiments and, thus, will be present as an impurity in the tokamak plasma [10].

2. Experiment

The experiment was set up at the electron-beam ion trap EBIT-2 at the Lawrence Livermore National Laboratory. Au ions were introduced into the trap from a metal vapor vacuum arc ion source (MeVVA). This ion source produces multiple, but not highly charged ions. The latter have to be produced from the ions initially caught in the trap by multiple collisions with the fast electrons of the high-current density electron beam. Ions become successively better trapped with increasing ion charge. Axial trapping is effected by drift-tube potentials, while radial trapping of the ions is due to a combination of the attraction by the electron beam, which also compensates the ion-cloud space charge, and by the very strongly reduced diffusion across the 3T magnetic guide field. electron-beam energies from 2400 to 5000 eV were employed to select specific maximum ion charge states up to Co-like Au^{52+}. The ions were kept inside the trap for about 5 s, then the trap was purged to prevent the accumulation of unwanted heavy contaminants. However, as the build-up phase is included in the observation, the spectrum comprises not only ions of the final charge state distribution (observed under quasi-steady state conditions for most of the cycle), but also lower charge state ions from the initial transient phase.

The light from the trapped ion cloud was observed by a flat-field spectrometer [11] equipped with a variable-line spacing grating having a 2400 lines/mm central line density and a cryogenic thinned, back-illuminated charge-coupled device (CCD) multichannel detector. The detector has 1024×1024 pixels of 25 μm pixel size. Along the spectrum 950 channels were evaluated, while across the dispersion direction the spectra — after filtering for cosmic ray spot events — were binned into three strips that were individually calibrated and analyzed. This procedure reduces the line broadening otherwise encountered by imaging errors (i.e., slight detector rotation and inherent line curvature) and offers additional consistency checks. Background spectra were subtracted from the data to account for the noise added to the data in the read-out process, nonuniformities introduced by thermal gradients across the CCD chip, and incidental light emanating from within EBIT. Typical observation times were 20 min per exposure. This is a compromise of long exposure times wanted for a good signal-to-noise ratio on one hand and the need to be able to recognize cosmic-ray events and correct for them on the other; with too many such events in an exposure, the filtering process may be less successful. Repeat exposures at various electron-beam energies ascertained the general reproducibility of the spectral features and their relative intensities.

[2] S.B. Utter et al. Manuscript in preparation.
[3] K.L. Wong et al. Manuscript in preparation.

Fig. 1. Sample spectra of Au in the wavelength range 30 to 60 Å. The electron-beam energy is indicated. Labels indicate the dominant charge state component (by isoelectronic sequence) of some of the lines.

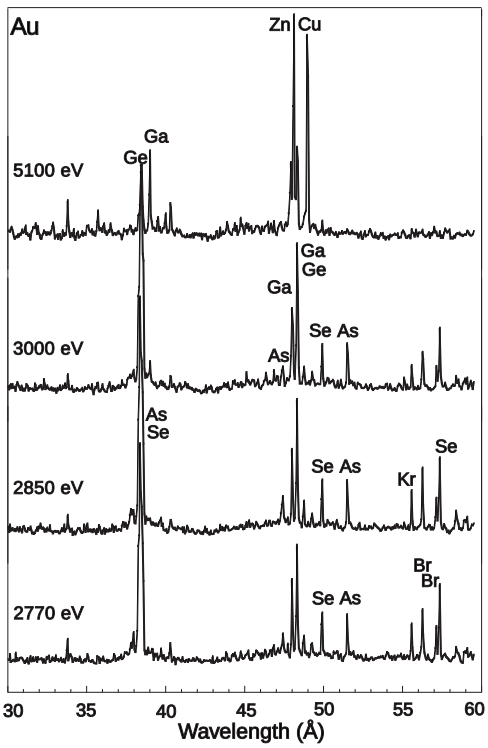

Fig. 2. Sample spectra of Au in the wavelength range 30 to 60 Å, for lower electron-beam energies than the spectra in Fig. 1. In the lowest electron energy spectra, the bulk of the strongest lines arises from charge states lower than Rb-like Au, for which presently no calculations are available.

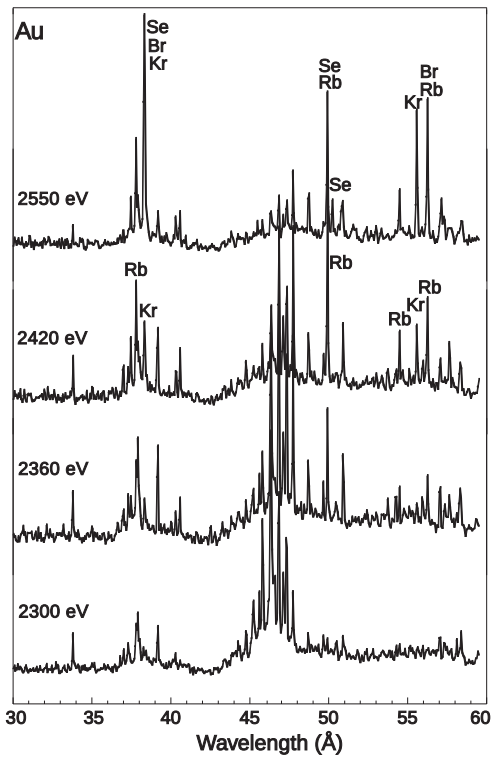

The spectra were recorded from about 10 to 60 Å in a single exposure. They were calibrated with the very well known 1s – 2p transitions in H-like and $1s^2$ – 1s2p and $1s^2$ – 1s3p transitions in He-like ions of C (33.736/40.268/34.973 Å), N (24.781/28.787/24.898 Å), and O (18.969/21.602/18.627 Å). Each of these is known to better than 1 mÅ. These lines were produced in dedicated spectra (without Au ion injection) at lower electron energies. The C, N, and O lines also showed as background in some of the Au spectra. At longer wavelengths in the spectral range of interest, several lines of Ne-like Ar (Ar^{8+}) were produced. The $2p^6\ ^1S_0 - 2p^5 3s\ ^{1,3}P^o_1$ transitions in this ion have wavelengths of 48.730 Å and 49.180 Å, respectively. These wavelengths have been determined to a precision of better than 5 mÅ [12]. In the EBIT spectra, a third line is partly blended with the second of the Ar lines, and is of practically equal intensity. The wavelength difference of 0.17 Å fits to the calculated level difference of the $2p^5 3s\ ^3P^o_1$ level to the $J = 2$ level [13]. Thus, an electric dipole (E1) and a magnetic quadrupole (M2) decay from the same level multiplet appear equally intense under EBIT operating conditions. A fourth Ne-like Ar line, a decay from a $2p^5 3d$ $J = 1$ level, appears fairly isolated at 41.480 Å. Outside of the range 18 to 50 Å, the wavelength scale has to rely on an extrapolation and consequently is less precise.

The wavelength calibration is better than 0.05 Å in the wavelength interval 20 to 50 Å. However, many of the strong lines in the Au spectra are blended with each other, so that some of the individual line positions cannot be determined with precision. In the long-wavelength interval 50 to 60 Å, more lines appear with isolated profiles, but the estimated uncertainty of the wavelength calibration degrades to almost 0.1 Å at the longest wavelengths. No reproducible spectral features of present interest were

Fig. 3. Collisional-radiative synthetic spectra for Ge-like Au^{47+} to Cu-like Au^{50+}.

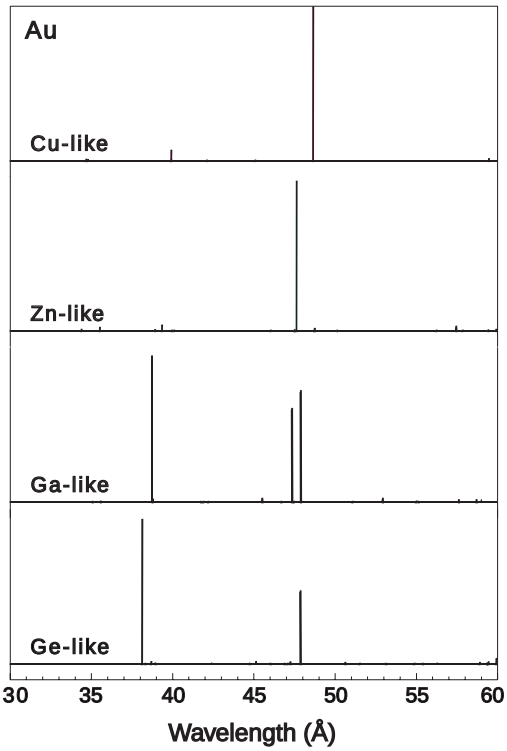

Fig. 4. Collisional-radiative synthetic spectra for Kr-like Au^{43+} to As-like Au^{46+}.

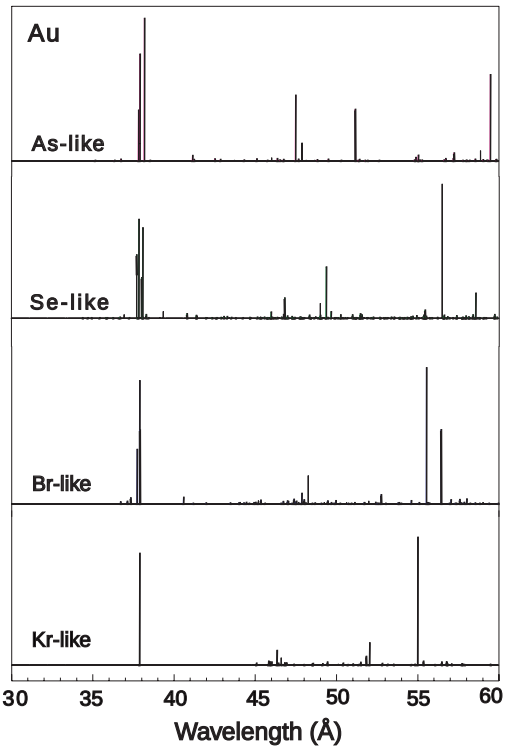

observed in the short-wavelength section below 35 Å, as was expected from the low spectral efficiency of the diffraction grating in that range. Furthermore, a notable spectral background appears at the short-wavelength end of the observed range and hampers the observation of weaker lines. The dispersion was calculated using a third-order polynomial fit to the calibration lines. Line widths (FWHM) varied along the spectral range, but generally were about 0.08 to 0.06 Å, which is not much more than the interval corresponding to the width of each CCD pixel. Examples of our spectra are shown in Figs. 1 and 2.

The reproducibility of the line positions in the three strips of each exposure and from one electron-beam energy setting to the next was usually better than 0.05 Å. In some series of spectra, line positions differ by one such step (one pixel size) that may relate to thermal instabilities of the spectroscopic set-up and thermal gradients across the CCD chip. The calibration uncertainty, however, is not the limiting factor for accurately analyzing the spectra. The most serious limitation was the fact that in several cases lines of various charge state ions appeared within a line width of others and could not be resolved well enough spectroscopically to obtain precise positions of the individual lines. In some cases, lines of three successive charge states appeared tightly blended and could not even be separated by the excitation curves. As the line width (FWHM) was rather close to a single pixel width, the 25 μm pixel size also posed a limit to spectral analysis.

3. Calculations

The present calculations aim simply at providing a guideline to the identity and wavelengths of the strongest (expected) lines of each ion and at estimates of relative intensities of neighboring lines. The calculations for Au in the present work followed the example of calculations for W that have recently been published elsewhere [14], which use a Maxwellian electron energy distribution to mimic

the temperature in a real plasma device. (In the present work, the electron-beam ion trap was used with fixed electron-beam energies, but at Livermore a technique has been developed to sweep the electron-beam energy in a pattern that, averaged over a cycle, yields a good approximation of a Maxwellian electron energy distribution [15].) The present calculations predict that most lines in our spectral range from the charge states of interest (Rb- to Ni-like) appear in two groups centered near 38 and 47 Å. At the lower electron-beam energies, low-charge state spectra are present that have not been modeled here.

Synthetic collisional-radiative spectra have been computed for Au^{42+} to Au^{52+}. The atomic data used to simulate the spectra have been generated with the HULLAC suite of codes [16–18]. Energy levels and E1, E2, M1, and M2 transition rates are computed with the fully relativistic parametric potential code RELAC [17]. Cross sections for the electron impact excitation of bound electrons are computed semi-relativistically in the distorted-wave approximation (DWA) [18]. All possible $\Delta n = 0$ (4–4) and $\Delta n > 0$ (3–4 and 3–5) excitations between singly excited levels have been considered. Some doubly excited configurations are included in the models to account for configuration interaction as fully as possible.

The distorted-wave cross sections are integrated over a Maxwellian distribution of free-electron energies to determine the final impact excitation rate coefficients. The electron impact excitation rate coefficients and the radiative transition probabilities are then entered into the collisional-radiative rate matrix. The relative populations for the levels of each ion are found in the steady state by solving the coupled set of rate equations:

$$n_j \left\{ \sum_{i<j}^{M} (A_{ji} + N_\mathrm{e} Q^\mathrm{d}_{ji}) + \sum_{k>j}^{M} N_\mathrm{e} Q^\mathrm{e}_{jk} \right\} = \sum_{k>j}^{M} n_k (A_{kj} + N_\mathrm{e} Q^\mathrm{e}_{kj}) + \sum_{i<j}^{M} n_i N_\mathrm{e} Q^\mathrm{d}_{ij} \qquad (1)$$

where n_j is the relative population of level j, Q_{ji} is the collisional rate coefficient from level j to level i for excitation (e) or de-excitation (d), A_{ji} is the radiative transition probability from level j to level i, and M is the number of levels used in the model for that ion. All electric and magnetic dipole and quadrupole radiative transitions (E1, M1, E2, and M2) as computed by RELAC are taken into account. Previous work with W spectra from these charge states has shown that dipole-forbidden transitions in this spectral range can be quite bright for the temperature-density conditions of the present experiments [10, 14]. The results of these calculations are summarized in Figs. 3 and 4.

The relative line intensities in the spectra simulated with a Maxwellian energy distribution might be closer to experimental findings from plasmas (with an electron energy distribution that can be described by a temperature) than to the present experimental EBIT data. Therefore, the synthetic spectrum of each ion was also computed integrating the DWA collision cross section, assuming an electron-beam with a Gaussian energy distribution of mean energy equal to the actual beam energies (indicated in Figs. 1 and 2) and with a full width at half maximum of 50 eV, representing an experimental electron beam with a finite energy spread. The relative strengths of the emission features in each ion are found to be nearly the same in the two simulations.

In our computation of the collisional-radiative spectrum of each ion, our model accounts for dipole-forbidden radiative channels and collisional depopulation of long-lived levels. Collisional destruction of the ground and excited levels in each ion through electron impact ionization has been neglected in these models. To compare the simulations to the experimental data in more detail, an approximation of the detector efficiency curve and a model of the mixture of charge states encountered in the EBIT would be required, but are not presently available.

4. Data and discussion

Data were recorded at electron-beam energies of 2300 eV (Br), 2360 eV (Se), 2420 eV (As), 2550 eV (Ge), 2770 eV (Ga), 2850 eV (Zn), 2900 eV (Zn), 3000 eV (Cu), 4800 eV (Ni), 4950 eV (Co), 5000 eV (Co), and 5100 eV (Co) (energies without correction for the space charge; the highest expected charge

Table 1. Lists of prominent lines observed in three electron-beam energy ranges (A: 4800 – 5100 eV; B: 2770 – 3000 eV; C: 2300 – 2550 eV) and suggested identifications based on observed production thresholds. Comments give rough relative intensities (s, strong; m, medium; w, weak); these categories are only for guidance, as some of the relative line intensities vary strongly with the electron-beam energy.

A: 4800 – 5100 eV Wavelength (Å)	Comment	B: 2770 – 3000 eV Wavelength (Å)	Comment	C: 2300 – 2550 eV Wavelength (Å)	Comment
33.75	w			33.75	w
35.68	w				
				36.94	w
				37.24	w
		37.42	w	37.42	m
37.95	vw	37.73/37.90	w	37.75	s
				37.87	m
				38.00	
38.26	s	38.24	s	38.26	s
38.40	s	38.35/38.49	s/s	38.36/38.60	m/w
		38.79	w		
38.96	m	38.95	w		
		39.12		39.11	m
39.40/39.50	w/w	39.62	w		
39.95	w				
40.27	w	40.27	w	40.26	w
				40.52	w
				44.71	w
45.06	w	45.07	w	45.05/45.20	m/m
				45.53	m
		45.72	w	45.75	m
				46.08	w
46.33	w	46.29	w	46.26	m
46.66/46.78	w/w	46.58	w	46.54/46.78	m/s
47.13	w			47.05	m
47.30	w	47.27/47.38	m/m	47.27	s
47.63/47.74	w/w	47.65	w	47.67	s
47.86	m	47.94	s		
48.05	s	48.05	s	48.1/48.15	w/w
48.28	m	48.25/48.32	s/m		
48.73	w	48.68	m	48.64	m
				48.85	w
48.92	s	48.92	m		
				49.10	w
				49.60	w
49.85	w	49.83	m	49.85	s
50.15/50.45	w/w	50.5	w	50.38	w
		50.74	w	50.83	m
51.4	w	51.43	s		
				52.30	w
53.3	w				
				53.63	w
				54.2/54.42/54.72	w/m/w
				55.03	w

Table 1. (*Concluded.)*

A: 4800 – 5100 eV Wavelength (Å)	Comment	B: 2770 – 3000 eV Wavelength (Å)	Comment	C: 2300 – 2550 eV Wavelength (Å)	Comment
55.5	w	55.46	m	55.44	s
				55.80	w
		56.15	s	56.2	w
		57.01	m	56.88	m
		57.20	s	57.15	w
		57.62	w	57.57	m
		58.22	w	58.15	w
		58.73/58.87	w		
		59.03/59.28	w		

state, identified by the isoelectronic sequence, is given in parentheses). Sample spectra are shown in Figs. 1 and 2, and wavelength results, grouped by high, medium, and low electron energy, are presented in Table 1. The observations confirm the general pattern of the predicted spectra. The individual wavelength predictions are good to about ± 0.5 Å, or about 1% of the transition's excitation energy. However, within such a range, several candidate lines are often found for each transition. Thus, a wavelength prediction on its own is not sufficient for line identification, and the variation of the line intensities with the electron-beam energy is needed to disentangle the experimental data.

Exceeding the production threshold of a given ion, however, does not imply that a spectral line from the newly reached charge state appears brightly enough to be recognized. For example, lines from Ni- and Co-like ions of Au, for which the highest electron energies used in this work should have just been sufficient, did in fact not show. One reason is that their predicted strongest lines are outside of the range of our efficient observation, that is they are on the short side of 30 Å. A second reason is that optimum production regularly happens at a few hundred eV above threshold, and such electron energies are often above one or more of the higher charge states' thresholds. This complicates the analysis, because lines that become prominent with increasing electron-beam energy regularly do not result from the highest charge state reached "in principle," but refer to ions of one or more charge states down. Only lines from ions in charge states that require higher production energies can be positively excluded — which is also helpful. This problem is aggravated by the actual pressure level (all in the UHV range) inside EBIT: it is difficult to reach the highest charge states with an imperfect vacuum, both for the energy loss experienced by the electrons and for the enhanced recombination rate of ions already trapped, which shifts the equilibrium charge state distribution. In the present study, spectral lines of a given ion charge state typically appear approximately 200 eV above the nominal threshold energies. This (expected) offset, however, is not necessarily the same for all ions and is not known precisely enough for deriving unequivocally the correct ion charge state. The charge state assignment that often implies a line assignment thus remains an iterative process. The results of this effort are listed in Table 2.

The high-electron-beam energy spectra are dominated by comparatively few lines near 48 Å, which are assigned as the 4s–4p resonance lines in Cu- and Zn-like ions. This finding agrees with the aforementioned detailed study of Cu- and Zn-like ions in the range $70 \leq Z \leq 92$, see footnote 2. In the middle electron-energy range, the dense line cluster near 38 Å can be ascribed to unresolved and superimposed multiplets of 4p–4d lines in As-, Se-, and Br-like ions. Isolated 4p–4d lines from Ge- and Ga-like ions appear in this spectral range in the higher beam energy spectra. The spectra are very rich for the lower electron-beam energies, with line clusters in the 46 to 47 Å and 49 to 60 Å ranges. Unfortunately, there are no peculiarities predicted that might be recognized in the spectra and thus give clues towards a reliable identification. For example, a single line near 49.9 Å features a maximum signal in spectra recorded at an electron-beam energy of about 2300 eV. This might suggest Kr-like

Table 2. Line identifications for ions of various isoelectronic sequences as based on observed production thresholds and available calculations. With the more complex configurations listed, there often are many levels with a given total angular momentum. An exact identification and specification would require a thorough isoelectronic analysis, for which no data are available. Identifications of strong lines refer to predicted strong lines. For weak lines (see Table 1), there are many more choices and possibly strong lines of other ionization stages that appear weakly under our excitation conditions. In this sense, our identifications of those weak lines are tentative. All wavelengths are from this work unless noted differently. *bl*, lines blended with others.

Ion	Isoel. seq.	Transition	Wavelength (Å) experiment	Wavelength (Å) theory
Au^{50+}	Cu	$3d^{10}4s\ J = 1/2 - 3d^{10}4p\ J' = 3/2$	48.92±0.01 48.9280 * 48.928 [19]	48.77
Au^{49+}	Zn	$3d^{10}4s^2\ J = 0 - 3d^{10}4s4p\ J' = 1$	48.05±0.01 48.0584 * 48.046 [20]	47.85 48.0 [23] 48.359 [24]RRPA 48.266 [24]MCRRPA 48.044 [24] semiemp. corr.
Au^{48+}	Ga	$4s^24p\ J = 1/2 - 4s^24d\ J' = 3/2$	38.95±0.02	39.00
		$4s^24p\ J = 1/2 - 4s4p^2\ J' = 1/2$	47.86±0.05	47.36
		$4s^24p\ J = 1/2 - 4s4p^2\ J' = 3/2$	48.28±0.05*bl*	47.90
Au^{47+}	Ge	$4s^24p^2\ J = 0 - 4s^24p4d\ J' = 1$	38.40±0.02*bl*	38.13
		$4s^24p^2\ J = 0 - 4s^24p^2\ J' = 1$	48.28±0.05*bl*	47.87
Au^{46+}	As	$4s^24p^3\ J = 3/2 - 4s^24p^24d\ J' = 1/2,3/2,5/2$	38.22 – 38.48*bl*	37.82 – 38.18
		$4s^24p^3\ J = 3/2 - 4s4p^4\ J' = 3/2$	47.94±0.05	47.49
		$4s^24p^3\ J = 3/2 - 4s4p^4\ J' = 5/2$	51.43±0.05	51.16
Au^{45+}	Se	$4s^24p^4\ J = 2,0 - 4s^24p4d\ J' = 1,2,3$	38.35 – 38.5*bl*	37.74 – 38.08
		$4s^24p^4\ J = 2 - 4s4p^5\ J' = 2$	49.85±0.05*bl*	49.38
		$4s^24p^4\ J = 2 - 4s^24p4d\ J' = 3$	57.20±0.08	56.51
Au^{44+}	Br	$4s^24p^5\ J = 3/2 - 4s^24p^44d\ J' = 1/2,5/2,3/2$	37.3 – 38.25*bl*	37.74 – 37.92
		$4s^24p^5\ J = 3/2 - 4s^24p^44d\ J' = 5/2,3/2$	56.15±0.08	55.54
		$4s^24p^5\ J = 3/2 - 4s^24p^44d\ J' = 5/2,3/2$	56.98±0.08 57.01±0.03	56.46
Au^{43+}	Kr	$4s^24p^6\ J = 0 - 4s^24p^54d\ J' = 1$	38.27±0.03	37.89
		$4s^24p^6\ J = 0 - 4s^24p^54d\ J' = 1$	55.46±0.08	55.01
Au^{42+}	Rb	$4s^24p^64d\ J = 3/2 - 4s^24p^54d^2\ J' = 3/2$	37.41±0.03	36.88
		$4s^24p^64d\ J = 3/2 - 4s^24p^54d^2\ J' = 1/2$	38.3*bl*	37.77
		$4s^24p^64d\ J = 3/2 - 4s^24p^54d^2\ J' = 5/2$	40.52±0.03	40.17
		$4s^24p^64d\ J = 3/2 - 4s^24p^64f\ J' = 5/2$	49.85±0.05*bl*	48.98
		$4s^24p^64d\ J = 3/2 - 4s^24p^54d^2\ J' = 1/2$	54.42±0.08	53.48
		$4s^24p^64d\ J = 3/2 - 4s^24p^54d^2\ J' = 3/2$	56.2±0.1	55.29
		$4s^24p^64d\ J = 3/2 - 4s^24p^54d^2\ J' = 5/2$	58.15±0.1	57.12

* See footnote 2.

ions (calculated threshold 2038 eV) or Rb-like ions (1977 eV) (or the nearby next few down) as the ion of origin. However, the calculations show no candidate line in Kr-like ions. The nearest predicted lines are from relatively weak transitions in Br-like ions (threshold 2274 eV) — both of which speaks against an identification — and a rather strong 4d–4f line predicted for Rb-like Au^{42+}, which makes this a likely candidate. No calculations were done for ions with more than 37 electrons that apparently dominate these low-electron energy spectra, but are too complex to attempt classification at this stage. Obviously, any spectroscopic observation with a spectral resolution that is poorer than that of the present experiment would not be able to gain much information from such rich spectra.

Comparisons with earlier data from laser-produced plasmas [19, 20] (which are supported by multiconfiguration Dirac–Fock calculations) are of limited use, as only the most prominent of the lines in Zn- and Cu-like ions given in that study appear in our spectra. This is probably due to the different (high-density there, low-density environment here) excitation process. In a dense plasma, an ion can be further excited (or de-excited) by collisions, reaching higher excitation states than in a single-step process. For an excited ion in a dilute plasma, radiative de-excitation to the ground state is much more likely than further collisional excitation. Our identification of the strong lines of Cu- and Zn-like ions is borne out by the two lines that survive to the highest energies used in the present work, right up to the threshold for opening up the outer shell of Ni-like ions. A similar situation as for Au ($Z = 79$) in this work has been found in a separate study of Cu-like lines of elements Yb, W, Au, Pb, Th, and U, see footnote 2. That systematic study, however, has reached a much higher wavelength precision than the present survey data permit.

While theory is less precise than our new experiments by a factor of 10 to 20, it is quite compatible with the isoelectronic trend of the experimental data. The codes used in the present work are an order of magnitude more accurate predicting the X-ray wavelengths of $\Delta n \neq 0$ transitions in these same ions, see footnote 3; the level of agreement reported on here is typical of HULLAC predictions for $\Delta n = 0$ transition wavelengths. Based on the present observations of prominent lines, calculations may now be scaled to provide better estimates for the multitude of presently unassigned less prominent lines, as well as to obtain reliable predictions for elements not yet covered by measurement. The present investigation extends earlier extreme-UV observations from foil-excited fast ion beams in which Ne- to Si-like ions of Au have been studied [21, 22]. In that experiment, only the Na-like ions were found to be adequately treated by calculation (to better than 1% for energies) and tested at the few-percent level for transition rates. The predictive power of theory was considered poorer for ions with additional $n = 3$ electrons. The present calculations for ions with filled $n = 3$ shells and several $n = 4$ electrons in an open shell, however, match the same level of precision.

This level of precision on its own, without experimental correction, is not sufficient for practical analyses of plasma spectra, for example with the aim of determining the charge balance. Typical plasma spectra so far have a poorer resolution than ours and, therefore, show wider features that result from superpositions of several lines each. Given the small wavelength differences between lines that are characteristic for specific charge states, a wavelength shift of 0.5 Å between experiment and theory can then easily lead to a misinterpretation of the contributing ion charge states by one or more units. However, the fact that so many prominent lines from different charge states coincide, at least for Au and probably some neighboring elements, renders possible an elemental analysis of a plasma from the apparent wavelengths of a few line clusters.

Acknowledgment

ET gratefully acknowledges travel support by the German Research Association (DFG) as well as the friendly hospitality of the LLNL EBIT group and of the colleagues at I.P.N.E., Université de Liège, Belgium, at various stages of this project. This project was performed under the auspices of the U.S. Department of Energy by the University of California Lawrence Livermore National Laboratory under Contract No. W-7405-Eng-48.

References

1. S. von Goeler, P. Beiersdorfer, M. Bitter, R. Bell, K. Hill, P. LaSalle, L. Ratzan, J. Stevens, J. Timberlake, S. Maxon, and J. Scofield. J. Phys. (Paris) Coll. C1, Suppl. au n^o 3, **49**, C1-181 (1988).
2. R. Neu, K.B. Fournier, D. Schlögl, and J. Rice. J. Phys. B **30**, 5057 (1997).
3. M.E. Foord, S.H. Glenzer, R.S. Thoe, K.L. Wong, K.B. Fournier, J.R. Albritton, B.G. Wilson, and P.T. Springer. J. Quantum Spectrosc. Radiat. Transfer, **65**, 231 (2000).
4. N. Tragin, J.-P. Geindre, P. Monier, J.-C. Gauthier, C. Chenais-Popovics, J.-F. Wyart, and C. Bauche-Arnoult. Phys. Scr. **37**, 72 (1988).
5. Y.-K. Kim. Phys. Scripta T, **73**, 19 (1997).
6. E. Träbert. *In* Accelerator-based atomic physics — techniques and applications. *Edited by* S.M. Shafroth and J.C. Austin. AIP, Washington. 1997. p. 567
7. M.A. Levine, R.E. Marrs, J.R. Henderson, D.A. Knapp, and M.B. Schneider. Phys. Scripta T, **22**, 157 (1988).
8. C.A. Back, D.H. Kalantar, R.L. Kauffman, R.W. Lee, B.J. MacGowan, D.S. Montgomery, L.V. Powers, T.D. Shepard, G.F. Stone, and L.J. Suter. Phys. Rev. Lett. **77**, 4350 (1996).
9. S.H. Glenzer, W. Rozmus, B.J. MacGowan, K.G. Estabrook, J.D. De Groot, G.B. Zimmerman, H.A. Baldis, J.A. Harte, R.W. Lee, E.A. Williams, and B.G. Wilson. Phys. Rev. Lett. **82**, 97 (1999).
10. K. Asmussen, K.B. Fournier, J.M. Laming, R. Neu, J.F. Seely, R. Dux, W. Engelhardt, J.C. Fuchs, and ASDEX Upgrade Team. Nucl. Fusion **38**, 967 (1998).
11. S.B. Utter, P. Beiersdorfer, G.V. Brown, E.J. Clothiaux, and N.K. Podder. Rev. Sci. Instrum. **70**, 284 (1999).
12. L.W. Phillips and W.L. Parker. Phys. Rev. **60**, 301 (1941).
13. A. Hibbert, M. Le Dourneuf, and M. Mohan. At. Data Nucl. Data Tables, **53**, 23 (1993).
14. K.B. Fournier. At. Data Nucl. Data Tables, **68**, 1 (1998).
15. D.W. Savin, P. Beiersdorfer, S.M. Kahn, B.R. Beck, G.V. Brown, M.F. Gu, D.A. Liedahl, and J.H. Scofield. Rev. Sci. Instrum. **71**, 3362 (2000).
16. A. Bar-Shalom and M. Klapisch. Comput. Phys. Commun. **50**, 375 (1988).
17. M. Klapisch, J. Schwob, B. Fraenkel, and J. Oreg. J. Opt. Soc. Am. **67**, 148 (1977).
18. A. Bar-Shalom, M. Klapisch, and J. Oreg. Phys. Rev. A: Gen. Phys. **38**, 1773 (1988).
19. J.F. Seely, C.M. Brown, and U. Feldman. At. Data Nucl. Data Tables, **43**, 145 (1989).
20. C.M. Brown, J.F. Seely, D.R. Kania, B.A. Hammel, C.A. Back, R.W. Lee, and A. Bar-Shalom. At. Data Nucl. Data Tables, **58**, 203 (1994).
21. E. Träbert, J. Doerfert, J. Granzow, R. Büttner, U. Staude, K.-H. Schartner, P. Rymuza, L. Engström, and R. Hutton. Z. Phys. D **32**, 295 (1995).
22. E. Träbert, U. Staude, P. Bosselmann, K.-H. Schartner, P.H. Mokler, and X. Tordoir. Euro. Phys. J. D **2**, 117 (1998).
23. L.J. Curtis. J. Opt. Soc. Am. B, **9**, 5 (1992).
24. T.-C. Cheng and K.-N. Huang. Phys. Rev. A, **45**, 4367 (1992).